JOURNAL OF CHEMICAL INFORMATION AND MODELING

Article

pubs.acs.org/jcim

Exploring the Molecular Mechanism of Cross-Resistance to HIV-1 Integrase Strand Transfer Inhibitors by Molecular Dynamics Simulation and Residue Interaction Network Analysis

Weiwei Xue,[†] Xiaojie Jin,[†] Lulu Ning,[†] Meixia Wang,[†] Huanxiang Liu,[‡] and Xiaojun Yao*[,†,§]

[†]State Key Laboratory of Applied Organic Chemistry, Department of Chemistry, [‡]School of Pharmacy, and [§]Key Lab of Preclinical Study for New Drugs of Gansu Province, Lanzhou University, Lanzhou 730000, China

Supporting Information

ABSTRACT: The rapid emergence of cross-resistance to the integrase strand transfer inhibitors (INSTIs) has become a serious problem in the therapy of human immunodeficiency virus type 1 (HIV-1) infection. Understanding the detailed molecular mechanism of INSTIs cross-resistance is therefore critical for the development of new effective therapy against cross-resistance. On the basis of the homology modeling constructed structure of tetrameric HIV-1 intasome, the detailed molecular mechanism of the cross-resistance mutation E138K/Q148K to three important INSTIs (Raltegravir (RAL, FDA approved in 2007), Elvitegravir (EVG, FDA approved in 2012), and Dolutegravir (DTG, phase III clinical trials)) was investigated by using molecular dynamics (MD) simulation and residue interaction network (RIN) analysis. The results from conformation analysis and binding free energy calculation can provide some useful information about the detailed binding mode and cross-resistance mechanism for the three INSTIs to HIV-1 intasome. Binding free energy decomposition analysis revealed that Pro145 residue in the 140s loop (Gly140 to Gly149) of the HIV-1 intasome had strong hydrophobic interactions with INSTIs and played an important role in the binding of INSTIs to HIV-1 intasome active site. A systematic comparison and analysis of the RIN proves that the communications between the residues in the resistance mutant is increased when compared with that of the wild-type HIV-1 intasome. Further analysis indicates that residue Pro145 may play an important role and is relevant to the structure rearrangement in HIV-1 intasome active site. In addition, the chelating ability of the oxygen atoms in INSTIs (e.g., RAL and EVG) to Mg^{2+} in the active site of the mutated intasome was reduced due to this conformational change and is also responsible for the cross-resistance mechanism. Notably, the cross-resistance mechanism we proposed could give some important information for the future rational design of novel INSTIs overcoming cross-resistance. Furthermore, the combination use of molecular dynamics simulation and residue interaction network analysis can be generally applicable to investigate drug resistance mechanism for other biomolecular systems.

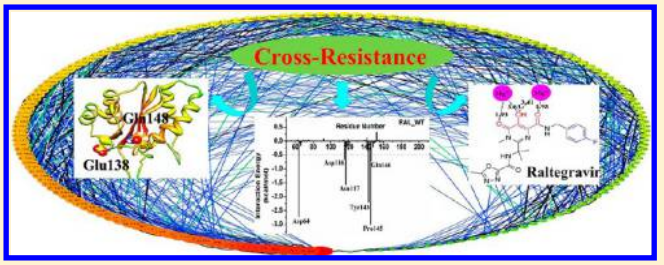

INTRODUCTION

Human immunodeficiency virus (HIV) is a retrovirus that causes acquired immunodeficiency syndrome (AIDS), and the successful highly active antiretroviral therapy (HAART) is the standard of care for patients with advanced infection.[1−5] HIV-1 integrase (IN) is an essential enzyme which catalyzes the integration of a viral DNA into the host cell genome and has been recently recognized as a promising therapeutic target for developing anti-AIDS agents.[6−8] HIV-1 IN enzyme consists of three discrete functional domains (Figure 1): the N-terminal domain (NTD, amino acids 1−49); the catalytic core domain (CCD, amino acids 50−212), and the C-terminal domain (CTD, amino acids 213−288).[9] The role of integration reaction promoted by IN involves two steps: 3′-processing and DNA strand transfer.[10,11]

In recent years, many integrase strand transfer inhibitors (INSTIs) with different chemical scaffolds have been developed (e.g., Raltegravir (RAL; MK-0518),[8,12] Elvitegravir (EVG; GS-9137),[13] and Dolutegravir (DTG; S/GSK1349572)[14,15]) and are well tolerated in HIV-1 infected individuals. The pyrimidinone carboxamide RAL (Figure 2A) is the first INSTI approved by the U.S. Food and Drug Administration (FDA) in 2007, which has significantly impacted AIDS therapy.[16] EVG (Figure 2B), a quinolone carboxylic acid, is recently approved by the FDA for the use in the treatment of HIV-1 infection in treatment-naïve adults.[17,18] While DTG (Figure 2C) is an advanced second-generation drug candidate in phase III clinical trials including treatment-naïve patients, and treatment-experienced, but integrase-naïve patients.[19] Given the potency and safety of INSTIs, RAL, EVG, and DTG have demonstrated effective activities against HIV-1 infection.[15,20,21] However, clinical resistance to these three INSTIs emerges rapidly and significant cross-resistance between these three agents has been reported recently.[14,22−24]

Among these cross-resistance mutations, the E138K/Q148K

Received: September 7, 2012
Published: December 11, 2012

dx.doi.org/10.1021/ci300541c | J. Chem. Inf. Model. 2013, 53, 210−222

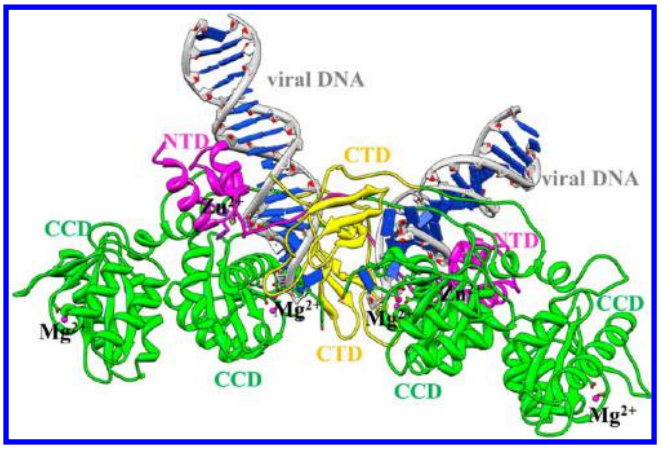

Figure 1. Structural model of a whole tetrameric HIV-1 intasome. HIV-1 IN and viral DNA are shown as ribbons. The N-terminal domain (NTD), C-terminal domain (CTD), and catalytic core domain (CCD) of the IN are colored in pink, yellow, and green. The Mg^{2+} and Zn^{2+} ions are presented as pink and gray spheres, respectively.

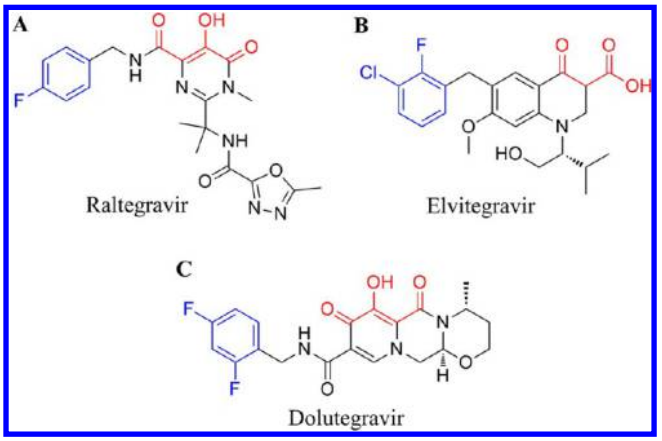

Figure 2. Chemical structures of the HIV-1 integrase strand transfer inhibitors (INSTIs) studied in this work. (A) Raltegravir (RAL; MK-0518). (B) Elvitegravir (EVG; GS-9137). (C) Dolutegravir (DTG; S/GSK1349572). The two-metal-chelating oxygen atoms and the halogenated phenyl group are illustrated in red and blue, respectively.

double mutant leads to a high-level resistance against RAL and EVG (fold changes (FCs), 330 and 371, respectively).[14] DTG demonstrates activity against clinically relevant IN mutant viruses and has a high genetic barrier to resistance. However, the E138K/Q148K mutant was still resistant to DTG (FCs, 19).[14] This double mutant can confer cross-resistance to INSTIs with diverse chemical scaffolds. Consequently, it is urgent and necessary to elucidate the detailed molecular mechanism of cross-resistance which will be helpful for the development of new potential INSTIs with a higher genetic barrier and limited drug resistance profiles.

The reported works on the drug resistance mechanism were mainly based on the structure of CCD of HIV-1 IN bound to inhibitors.[25−29] However, several lines of evidence suggest that the tetrameric HIV-1 intasome, comprised by the IN enzyme and the end of the viral DNA, is the basic recombination unit of HIV-1 integration.[30−32] The clinically useful INSTIs selectively interact with the intasome rather than free integrase.[30−32] INSTIs (e.g., RAL, EVG, and DTG) occupy the active site of the HIV-1 intasome and block the access of the host cell genome to integrate.[32,33] Therefore, this common mechanism of action for INSTIs may have important implications for exploring the binding mode and cross-resistance mechanism.[34] It is more reasonable to study the binding mode and drug resistance mechanism of the INSTIs based on the structure of the intasome. Understanding how HIV-1 intasome mutations lead to cross-resistance against INSTIs is still a complicated problem and great challenge since the experimental determined structural information of the HIV-1 intasome remains elusive. However, recent determination of the prototype foamy virus (PFV) IN crystal structures in the presence of INSTIs and viral DNA suggests that INSTIs inhibit the function of IN by binding within the active site of PFV intasome.[35] Thus, due to the fact that the amino acid sequence of PFV IN with HIV-1 IN demonstrates high conservation in the key structural elements, it is possible to build the structure of HIV-1 intasome from the structure of PFV intasome. The reported works proved that the modeled structure of intasome would be very helpful to the development of antiretroviral drugs.[19,32,33,36−39] The study of the cross-resistance mechanism of INSTIs is critical for the development of effective therapies targeting the drug resistant strains and study the cross-resistance mechanism of INSTIs from the structure of tetrameric HIV-1 intasome would be more reasonable and reliable.[19,40]

In the present work, we attempt to elucidate the molecular mechanism of cross-resistance to three different HIV-1 INSTIs from the structures of the constructed complex of tetrameric HIV-1 intasome with INSTIs. The structural model of tetrameric HIV-1 intasome in complex of INSTIs were constructed by homology modeling and further investigated via molecular dynamics (MD) simulation. On the basis of the MD-simulated structures, an approach by the combination use of binding free energy calculation and residue interactions network (RIN) analysis was performed to gain insight into the cross-resistance mechanism. The MD simulation is capable of revealing the conserved binding mode for INSTIs and conformational changes of the complexes due to the E138K/Q148K double substitution. While the calculated binding free energy and energy decomposition analysis help us to understand the detailed interaction profiles of the INSTIs with wild-type (WT) and mutant. Moreover, the RIN analysis of the intasome can provide some information about the residue interactions to discover possible mechanisms of drug resistance. As a result, the method here to combine the advantages of the MD simulation, binding free energy calculation, and network analysis approaches can be effective to study the cross-resistance mechanism. More importantly, the insights from our study may have a crucial application in designing novel INSTIs as potent and less cross-resistance anti-AIDS agents.

METHODS

System Setup. The initial coordinate for the WT HIV-1 IN was taken from our previous constructed structure.[33] Herein, we used the structure-based alignment of PFV and HIV-1 IN to get the structure of HIV-1 intasome tetramer in complex with Mg^{2+} ions and INSTIs. First, the transformation matrices method in VMD (v1.87)[41] was applied to build the PFV IN tetramer. Subsequently, the resulting tetrameric structure was used to generate HIV-1 IN tetramer and introduce viral DNA, Mg^{2+} ions, and INSTIs from the PFV structures (PDB ID code 2OYA,[35] 3L2U,[35] and 3S3M[42] for RAL, EVG, and DTG bound complexes, respectively) to the correct position of HIV-1 IN tetramer by program Swiss-PdbViewer (v4.0.4)[43] using the C_α

dx.doi.org/10.1021/ci300541c | J. Chem. Inf. Model. 2013, 53, 210−222

positions of active site residues Asp64, Asp116, and Glu152 from the CCD. In addition, the 19-base-pair mimic of preprocessed terminal viral DNA from the PFV structure was mutated to HIV-1 viral DNA based on the sequence alignment.[32] Finally, PyMOL software (v0.99rc6)[44] was applied to generate the 3D structures of the studied tetramer of HIV-1 intasome mutants (E138K/Q148K) by substituting specific residues using the WT intasome model as the template.

The LEaP module of the Amber10 package[45] was used for the addition of all missing hydrogen atoms. Then, each system was immersed into a rectangular periodic box with at least 10 Å distance around the complex, containing approximately 57000 TIP3P[46] water molecules previously equilibrated by Monte Carlo methods. The appropriate numbers of sodium counterions were included to maintain electroneutrality. The standard Amberff03 force field[47] was selected for describing the enzyme, viral DNA as well as the parameters for Mg^{2+}. Zinc binding to the N-terminal domain was assigned a formal charge of +2.0 and a van der Waals radius of 1.10 Å according to previously derived parameters.[48]

Parametrization of INSTIs. The force field parameters for RAL, EVG, and DTG were created with the use of the Antechamber program from the Amber10 package, using general Amber force field (GAFF)[49] and restrained electrostatic potential (RESP)[50−52] partial charges. Geometric optimization and the electrostatic potential calculations were performed at the HF/6-31G* level of Gaussian09 suite.[53]

Molecular Dynamics Simulation. All molecular dynamics simulations were performed using Amber10 package. The energy minimization and equilibration protocol was carried out with the Sander program. First, each system was minimized by two steps, applying harmonic restraints with a force constant of 500.0 kcal/(mol·Å^2) to all protein atoms and allowing all atoms to move freely in turn. In each step, energy minimization was performed by the steepest descent method for the first 3000 steps and the conjugated gradient method for the subsequent 2000 steps. And then, the energy minimization was followed by heating from 0 to 300.0 K over 50 ps in the *NVT* ensemble and equilibrating to adjust the solvent density under 1 atm pressure over 50 ps in the *NPT* ensemble simulation by restraining all atoms of the structures with a harmonic restraint weight of 10.0 kcal/(mol·Å^2). An additional three MD equilibrations of 50 ps each were performed with the decreased restraints weight from 5.0, to 1.0, to 0.1 kcal/(mol·Å^2), respectively. These were followed by the last MD equilibration step of 50 ps by releasing all the restraints.

Afterward, 20 ns production MD simulations were carried out with PMEMD program without any restraint on these three systems in the *NPT* ensemble at a temperature of 300.0 K and a pressure of 1 atm. A time step of 2 fs was used for the equilibration stages and production simulations. During the simulations, periodic boundary conditions were employed and all electrostatic interactions were calculated using the particle-mesh Ewald (PME) method[54] with a dielectric constant of unity. For all simulations, a 12.0 Å cutoff was used to calculate the direct space sum of PME, and bond lengths involving bonds to hydrogen atoms were constrained using the SHAKE algorithm.[55]

Thermodynamic Calculation. The binding free energy of the INSTIs (RAL, EVG, and DTG) to the HIV-1 intasome was analyzed by molecular mechanics generalized born surface area (MM-GBSA)[56−59] method, integrated in the Amber10 package. This method has been used successfully to study a wide variety of problems.[60−67] The first step of MM-GBSA is to generate multiple snapshots from the stable MD production trajectory of the complex. Here, 1000 snapshots were extracted from each MD trajectory from last 5 ns, equally spaced at 5 ps intervals. For each snapshot, a free energy is calculated for each molecular species (complex, receptor, and ligand), and the ligand binding free energy is estimated as follows:

$$\Delta G_{\text{bind,GB}} = G_{\text{complex,GB}} - G_{\text{receptor,GB}} - G_{\text{ligand,GB}} \quad (1)$$

where $G_{\text{complex,GB}}$, $G_{\text{receptor,GB}}$, and $G_{\text{ligand,GB}}$ are the free energy of complex, receptor, and ligand molecules, respectively. The free energy ($G_{\text{bind,GB}}$) was calculated based on an average over the extracted snapshots from a single-trajectory MD simulation. Each state is estimated from the molecular mechanics energy E_{gas}, the solvation free energy $G_{\text{sol,GB}}$, and the solute entropy S, respectively.

$$G_{\text{bind,GB}} = E_{\text{gas}} + G_{\text{sol,GB}} - TS \quad (2)$$

$$E_{\text{gas}} = E_{\text{int}} + E_{\text{vdW}} + E_{\text{ele}} \quad (3)$$

$$G_{\text{sol,GB}} = G_{\text{GB}} + G_{\text{sol-np,GB}} \quad (4)$$

$$G_{\text{sol-np,GB}} = \gamma \text{SASA} \quad (5)$$

where E_{gas} is the gas-phase energy; E_{int} is the internal energy; E_{ele} and E_{vdW} are the Coulomb and van der Waals energies, respectively. E_{gas} was calculated using the Amberff03 force field. $G_{\text{sol,GB}}$ is the solvation free energy and can be decomposed into polar and nonpolar contributions. G_{GB} is the polar solvation contribution calculated by solving the GB equation. Dielectric constants for solute and solvent were set to 1 and 80, respectively. $G_{\text{sol-np,GB}}$ is the nonpolar solvation contribution and was estimated by the SASA determined using a water probe radius of 1.4 Å. The surface tension constant γ was set to 0.0072 kcal/(mol·Å^2).[68] T and S are the temperature and the total solute entropy, respectively. Vibrational entropy contributions can be estimated by classical statistical thermodynamics, using normal-mode analysis.[69] As our aim is not to obtain the absolute Gibbs energy but to analyze the detailed interaction features, the entropy contribution was not included in this study due to the difficulty and complexity to calculate entropy accurately from normal-mode analysis for such large protein−ligand complexes.

Per-residue Free Energy Decomposition Analysis. The inhibitor−residue interaction is valuable to qualitatively describe the binding mode of RAL, EVG, and DTG to HIV-1 intasome. Given the pairwise nature of the GB equation allowing the decomposition of polar solvation energy (ΔG_{GB}) into atomic contributions in a straightforward manner, the interaction between an inhibitor and each residue was computed using the MM-GBSA decomposition process in Amber10 without considering the contribution of entropies by

$$G_{\text{inhibitor-residue,GB}} = E_{\text{vdW}} + E_{\text{ele}} + G_{\text{GB}} + G_{\text{sol-np,GB}} \quad (6)$$

where E_{vdW} and E_{ele} are nonbonded van der Waals interactions and electrostatic interactions were computed using the Sander program in Amber10. G_{GB} and $G_{\text{sol-np,GB}}$ are the polar and nonpolar contributions to the inhibitor−residue interaction. The polar solvation contribution (G_{GB}) was calculated by using the generalized Born (GB) model,[70] and the parameters for the GB calculation were developed by Onufriev et al. (GB^{OBC}, igb = 2). The nonpolar contribution of desolvation ($G_{\text{sol-np,GB}}$) was computed based on SASA. All energy components were

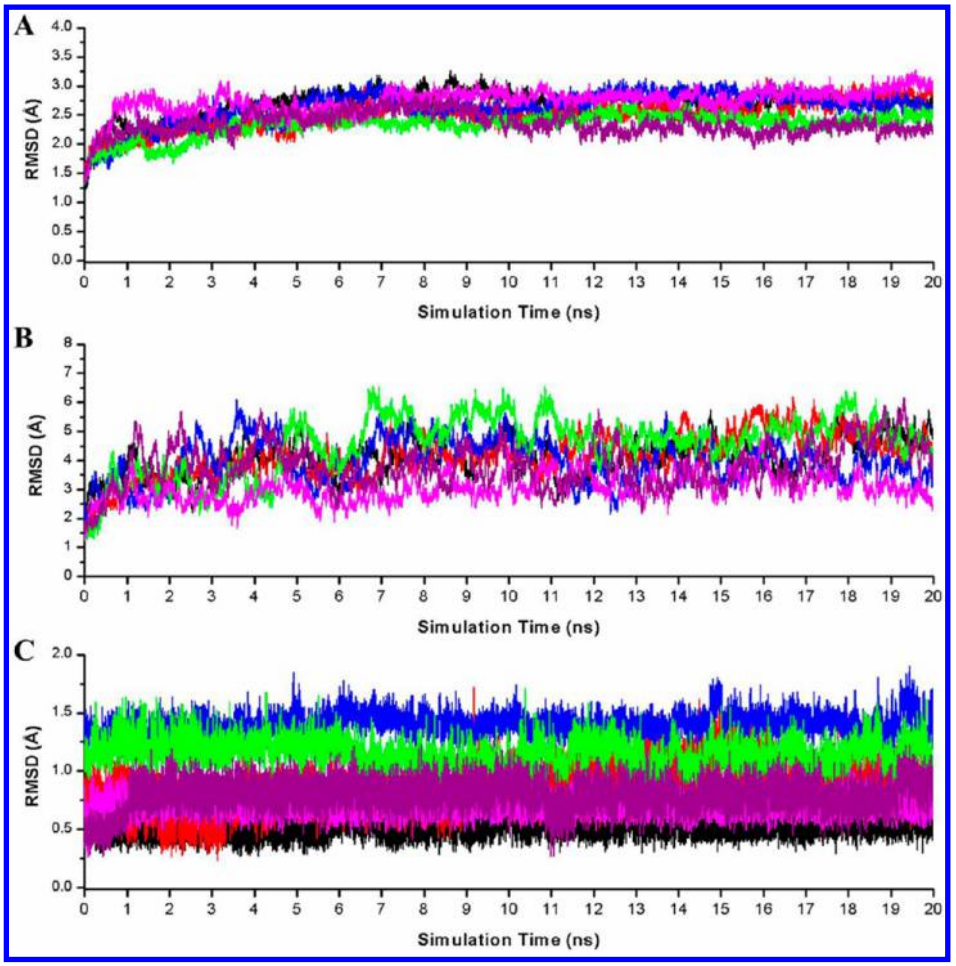

Figure 3. Monitoring of the equilibration of the MD trajectories for each system. (A) Time evolution of the root mean squared deviation (RMSD) of backbone atoms for HIV-1 IN CCD. (B) Time evolution of the RMSD of backbone atoms for viral DNA. (C) Time evolution of the RMSD of heavy atoms for the INSTIs. The six simulations of RAL, EVG, and DTG bound to the WT and E138K/Q148K mutant complexes are represented in black, red, blue, green, pink, and purple, respectively. The values reflect the equilibration of each of the systems relative to the initial structures.

calculated using 1000 snapshots collected from the last 5 ns MD simulation trajectory .

Residue Interaction Network Calculation. The average structure derived from the last 5 ns MD simulation trajectory of each system was used for constructing the residue interaction network (RIN). The REDUCE[71] program was applied for accurately adding hydrogen atoms. The resulting structural models with hydrogen atoms were used in PROBE,[72] in order to identify noncovalent residue between the atoms of each pair of considered residues and defines the two residues as in contact if between any of their atoms exists at least one van der Waals interaction. Cytoscape[73] and the plugin RINalyzer[74] were used to visualize the residue interaction network with protein residues and their noncovalent interactions represented by nodes and edges, respectively. Using the NetworkAnalyzer[75] plugin of Cytoscape, we calculated the node degree in the network as the number of edges linked to a specific node within an undirected network, as well as the node connectivity which is the number of its interactions with neighboring nodes. Herein, to perform the weighted centrality measurement, we also compute shortest path closeness using the plugin RINalyzer.

RESULTS AND DISCUSSION

Structures and Binding Mode Simulation Results for the HIV-1 Intasome in Complex with INSTIs. Due to the low solubility in solutions, it is difficult to obtain the 3D structure HIV-1 intasome experimentally.[76] However, Cherepanov et al reported the crystal structure of the PFV IN contains INSTIs bound in the presence of viral DNA and Mg^{2+} ions.[35,42] Therefore, we constructed the whole structure of tetrameric HIV-1 intasome (Figure 1) in complex with three INSTIs based on the crystal structure of PFV intasome. The modeled binding mode of INSTIs to HIV-1 intasome conserved active site is extremely similar to that of the PFV intasome crystal structures.

In order to obtain additional insight into the binding mode of the three INSTIs, we carried out 20 ns MD simulation on tetrameric HIV-1 intasome in complex with RAL, EVG, and DTG in explicit solvent. The root-mean-square deviation (RMSD) of each snapshot relative to the initial structure was calculated to monitor the stability of each trajectory. Here, we mainly focus on the active site of intasome. On the basis of the binding mode of the tetrameric complex, the RMSD of the MD-simulated structures, including the HIV-1 IN CCD (amino acids 50−212), viral DNA, and INSTIs (e.g., RAL, DTG, and EVG) are plotted as a function of time in Figure 3. As shown in Figure 3, the RMSD of all the trajectories remains constant

dx.doi.org/10.1021/ci300541c | J. Chem. Inf. Model. 2013, 53, 210−222

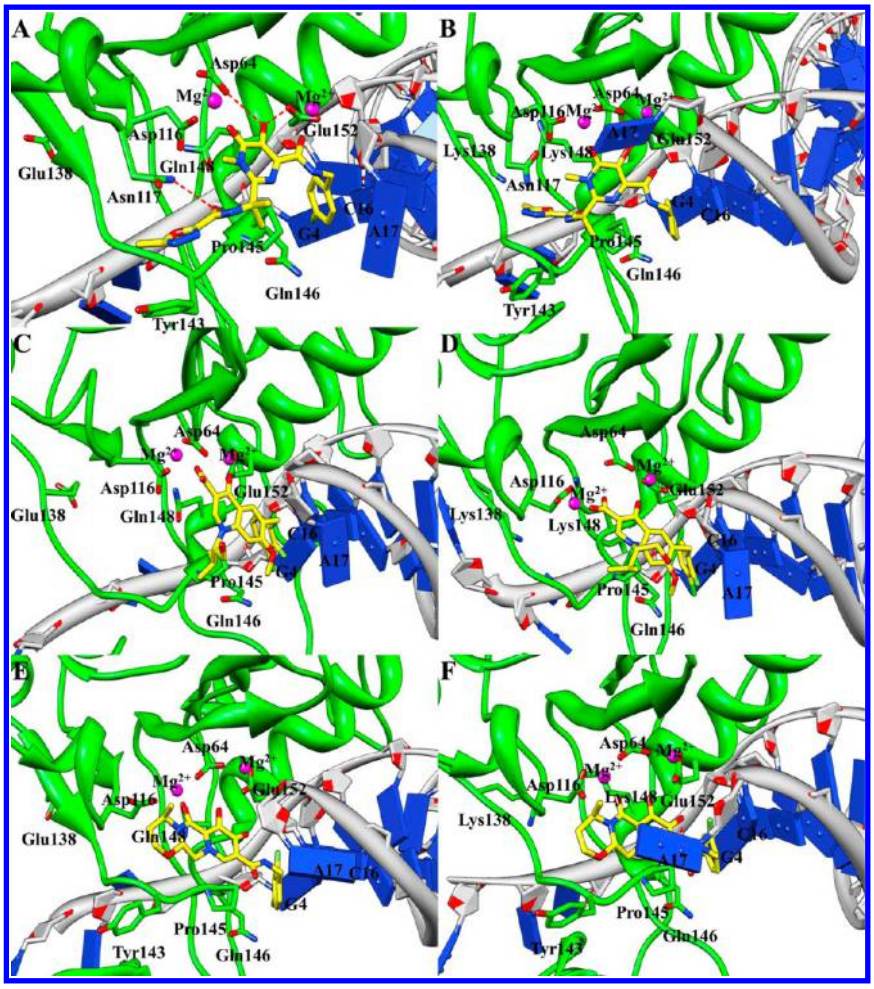

Figure 4. MD-simulated structure of RAL, EVG, and DTG bound to the WT and E138K/Q148K HIV-1 intasome active site (A–F). IN and viral DNA are represented as green and gray ribbon, respectively. Green stick representations are shown for residues in the intasome active site. INSTIs are shown as a yellow stick representation, and Mg^{2+}, as pink spheres. Red dashed lines represent the hydrogen bond.

during the 20 ns of MD simulation, indicating the stability of the studied complexes. The trajectory of last 5 ns simulations was taken for the following structural and energetic analysis.

The simulated average conformations of the active site for the WT and E138K/Q148K double mutant HIV-1 intasome/INSTIs complex over the last 5 ns simulation was shown in Figure 4. The simulation results indicate that INSTIs bind to a pocket formed by the flexible 140s loop (e.g., residues from Gly140 to Gly149) and the 5′-CA overhang of the viral DNA. This conserved binding mode of INSTIs in the WT model could give some information about the essential pharmacophore (the chelating and hydrophobic moieties of INSTIs highlighted in Figure 2) observed in several experimental studies.[77−80] Usually, hydrogen bonds play an essential role in stabilizing the protein−ligand complexes. As can be seen in Figure 4A, RAL mainly forms hydrogen bonds with Asp64, Asn117, and Glu152 in the WT model. Whereas the hydrogen bonds between RAL and Asn117 (Glu152) disappeared in the E138K/Q148K mutant due to the conformation rearrangement of HIV-1 intasome active site. In addition, the mutation significantly altered the crucial face-to-face $\pi-\pi$ stacking of RAL with Tyr143 (Figure 4A and B). The monitored distances between the centroid of INSTIs scaffold and Pro145 in the WT and E138K/Q148K mutant HIV-1 intasome−INSTIs complexes (Table S1, Supporting Information) have shown that INSTIs scaffold form a more close hydrophobic interaction with Pro145 (Figure 4B, D, and F) in the E138K/Q148K mutant intasome than that in the WT complex (Figure 4A, C, and E). It demonstrate that the strong hydrophobic interactions between the side chain of Pro145 and INSTIs is critical to keep the INSTIs in a right conformation to accommodate the HIV-1 intasome active site. Additionally, the results from reported experimental[35,42,81] and theoretical[33,39] studies have pointed out the critical role of the 3′ adenosine's (A17) flip directing INSTIs into the binding site of intasome. For RAL-bound HIV-1 intasome, the 3′ adenosine underwent significant conformational change in the in the E138K/Q148K complex (Figure 4B) compared to that in the WT structure (Figure 4A). Moreover, this conformational change causes the decomposed binding free energy contributions from residues A17 decreased (Figure S1A and B, Supporting Information). We further analyzed the poses of EVG- and DTG-bound HIV-1 intasome. The position of 3′ adenosine (A17) is not significantly influenced by this drug resistance mutation (Figure 4C−F). There is no significant change in the size of the decomposed binding free energy contribution from residue A17 when compared to the complex formed by WT intasome with EVG or DTG (Figure S1C−F, Supporting Information).

Figure 5 further illustrates the details about the interaction of INSTIs with two Mg^{2+} ions (two-metal-chelating mode) in the

dx.doi.org/10.1021/ci300541c | J. Chem. Inf. Model. 2013, 53, 210−222

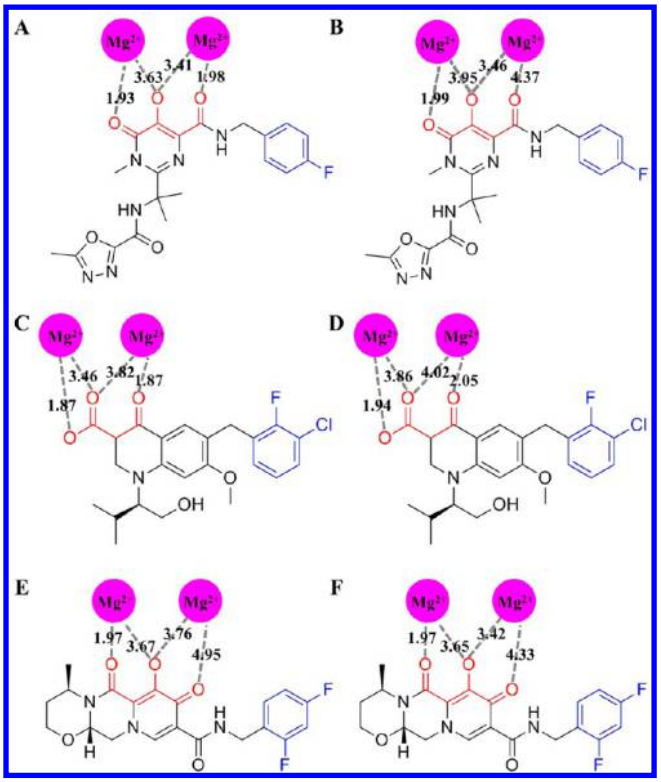

Figure 5. Scheme of two-metal-chelating mode for HIV-1 INSTIs (A) RAL, (B) EVG, and (C) DTG. The two-metal-chelating oxygen atoms are illustrated in red and coordinate to the active site Mg^{2+} ions (pink sphere) with the bonds between the INSTIs and Mg^{2+} ions shown as dashed gray lines.

active site of intasome. The two-metal-chelating mode concept was proposed in 2001[82] and proved to be an important strategy for the design of new and potent INSTIs.[83−87] However, the metal binding atoms in this study are not the same since the binding atoms including different combinations of carbonyl and phenolic oxygen atoms (Figure 5). The measured distance (labeled in red) between the Mg^{2+} ions and INSTIs (RAL and EVG) oxygen atoms in the E138K/Q148K HIV-1 intasome active site is 4.37 and 2.05 Å respectively (Figure 5B and D), unlike its WT interaction mode shown in Figure 5A and C. This significant difference in the ability of oxygen atoms to chelate Mg^{2+} has important influence on the binding mode of these compounds to the active site of HIV-1 intasome. In contrast, it is notable that the predicted two-metal-chelating mode in DTG bound complexes shows similar chelating ability with the WT intasome, which is consistent with the lower cross-resistance potential of DTG observed from the experimental data.[14] In addition, this can also explain the overlapping resistance investigated among the first-generation agents RAL and EVG in vitro and in vivo that owing to the common manner in which INSTIs engage the Mg^{2+} within the HIV-1 intasome active site.[34] Moreover, comparison of the structure of the three INSTIs (Figure 2) indicates that RAL and EVG possess a more flexible linker region which dictates the angle and distance between the between the metal chelating core and the halogenated phenyl moiety. Therefore, further rational drug design the attention should be focused on the scaffold optimization of bond angles between the oxygen atoms[87] and linker region of the compound.[37,42,88]

Thermodynamic Analysis. *(1) Binding Free Energy Calculation.* As a complement to the binding mode and structural information discussed above, estimation of the binding free energy of RAL, EVG, and DTG to the WT HIV-1 intasome and its E138K/Q148K mutant obtained from the MM-GBSA calculation are shown in Table 1. Binding free energy profiles could provide useful insight into the inhibitor binding mechanism followed by individual contributions to the binding free energy. According to Table 1, the calculated contributions favoring binding are the electrostatic interactions (ΔE_{ele}) between the binding partners, ranging from −57.12 to −119.04 kcal/mol, and the intermolecular van der Waals energy (ΔE_{vdW}) ranging from −33.26 to −45.34 kcal/mol for all HIV-1 intasome−INSTIs complexes. Nonpolar polar solvation terms ($\Delta G_{sol\text{-}np,GB}$, ranging from −5.00 to −6.56 kcal/mol), which correspond to the burial of solvent accessible surface area (SASA) upon binding, contribute slightly favorably. By contrast, the polar solvation contribution (ΔG_{GB}, ranging from 80.30 to 131.45 kcal/mol) has unfavorable contribution to the binding. Overall, the total binding free energy ($\Delta G_{bind,GB}$) predicted for RAL, EVG, and DTG binding with the HIV-1 intasome are different, with values ranging from −16.15 to −30.95 kcal/mol. In addition, to explore binding free energy change caused by the double mutation, the results of INSTIs bound to the WT and mutant HIV-1 intasome are reported as relative resistance binding free energy $\Delta\Delta G^{calc}_{bind}$ as shown in Table 2. For comparison with the theoretical computation, the experimental fold changes (FCs) were also converted to $\Delta\Delta G^{exe}_{bind}$ (Table 2). The results proved that the present

Table 1. Calculated Binding Free Energy Terms and Experimental Fold Changes (FCs) for RAL, EVG, and DTG Binding to the WT and E138K/Q148K Mutant HIV-1 Intasome

	RAL		EVG		DTG	
contribution[a]	WT	E138K/Q148K	WT	E138K/Q148K	WT	E138K/Q148K
ΔE_{ele}	−57.12 (0.18)	−57.33 (0.17)	−105.00 (0.67)	−119.04 (0.28)	−77.23 (0.17)	−88.73 (0.19)
ΔE_{vdW}	−40.83 (0.11)	−45.34 (0.13)	−33.73 (0.14)	−33.26 (0.13)	−42.65 (0.12)	−39.56 (0.13)
ΔE_{gas}	−97.96 (0.17)	−102.67 (0.15)	−138.73 (0.57)	−152.30 (0.25	−119.87 (0.15)	−128.29 (0.15)
$\Delta G_{sol\text{-}np,GB}$	−6.26 (0.0063)	−6.56 (0.0072)	−5.00 (0.0098)	−5.61 (0.0082)	−5.97 (0.0047)	−6.31 (0.0038)
ΔG_{GB}	83.30 (0.28)	93.08 (0.11)	113.57 (0.41)	131.45 (0.21)	94.90 (0.10)	107.45 (0.12)
$\Delta G_{sol,GB}$[b]	77.05 (0.28)	86.52 (0.11)	108.57 (0.42)	125.84 (0.21)	88.92 (0.10)	101.14 (0.12)
$\Delta G_{ele,GB}$[c]	26.18 (0.26)	35.76 (0.10)	8.57 (0.28)	12.41 (0.13)	17.67 0.11)	18.72 (0.11)
$\Delta G_{bind,GB}$[d]	−20.91 (0.24)	−16.15 (0.11)	−30.16 (0.18)	−26.46 (0.11)	−30.95 (0.10)	−27.15 (0.10)
FCs[e]	1.0	330	1.0	371	1.0	19

[a]All energies are in kilocalories per mole, with corresponding standard errors in parentheses. [b]$\Delta G_{sol,GB} = \Delta G_{sol\text{-}np,GB} + \Delta G_{GB}$. [c]$\Delta G_{ele,GB} = \Delta G_{GB} + \Delta E_{ele}$. [d]$\Delta G_{bind,GB} = \Delta E_{ele} + \Delta E_{vdW} + \Delta G_{sol,GB}$. [e]FCs is defined as EC_{50}(E138K/Q148K)/EC_{50}(WT) in ref 14.

dx.doi.org/10.1021/ci300541c | J. Chem. Inf. Model. 2013, 53, 210−222

Table 2. Summary of Theoretical and Experimental $\Delta\Delta G_{bind}$[a] Values for the WT and E138K/Q148K Mutant HIV-1 Intasome−INSTIs Complexes

system	RAL	EVG	DTG
$\Delta\Delta G_{bind}^{calc}$ [b]	4.76	3.70	3.80
$\Delta\Delta G_{bind}^{exe}$ [c]	3.43	3.41	1.74

[a]All results are given in kilocalories per mole. [b]The relative binding free energy ($\Delta\Delta G_{bind}$) for the WT and E138K/Q148K mutant HIV-1 intasome−INSTIs complexes is defined as $\Delta\Delta G_{bind} = \Delta G_{bind}^{E138K/Q148K} - \Delta G_{bind}^{WT}$. [c]The experimental values $\Delta\Delta G_{bind}^{exe}$ were derived from the experimental FCs values in the references by using the equation $\Delta\Delta G_{bind}^{exe} \approx RT \ln(FCs)$ at 300.0 K.

theoretical calculations agree well with the referenced experimental values.

(2) Spectrum of the Residue Interaction Contributions. To obtain a more detailed thermodynamic description of the residue contributions to the binding free energy, we decomposed the $\Delta G_{bind,GB}$ value on a per-residue level depicted in Figure 6 and Figure S1 (Supporting Information), in which the interactions included the contributions from side chains and the backbone of the residues. On the basis of the individual residue contribution to the interaction energy, we identified the common residues contribute to the binding of RAL, EVG, and DTG are as follows: Asp64, Asp116, Pro145, Gln146, Glu152, G4, C16, and A17. As can be seen from Figure 6 and Figure S1 (Supporting Information), their contributions to the interaction energy vary from −0.42 to −5.24 kcal/mol.

By comparing the individual residue contribution to the binding free energy of INSTIs bound WT and E138K/Q148K systems (Figure 6 and Figure S1 (Supporting Information)), we analyzed the molecular basis of the difference between the potency changes of RAL, EVG, and DTG. We found that the contributions from residues Asp64, Asp116, Asn117, Tyr143, and A17 are decreased in RAL bound mutant. In contrast, the contributions from residues Glu152, G4, and C16 are increased. While for EVG, there is also significant change in the size of the individual residue contribution compared to the WT for this mutant. The mutation causes the contributions from residues

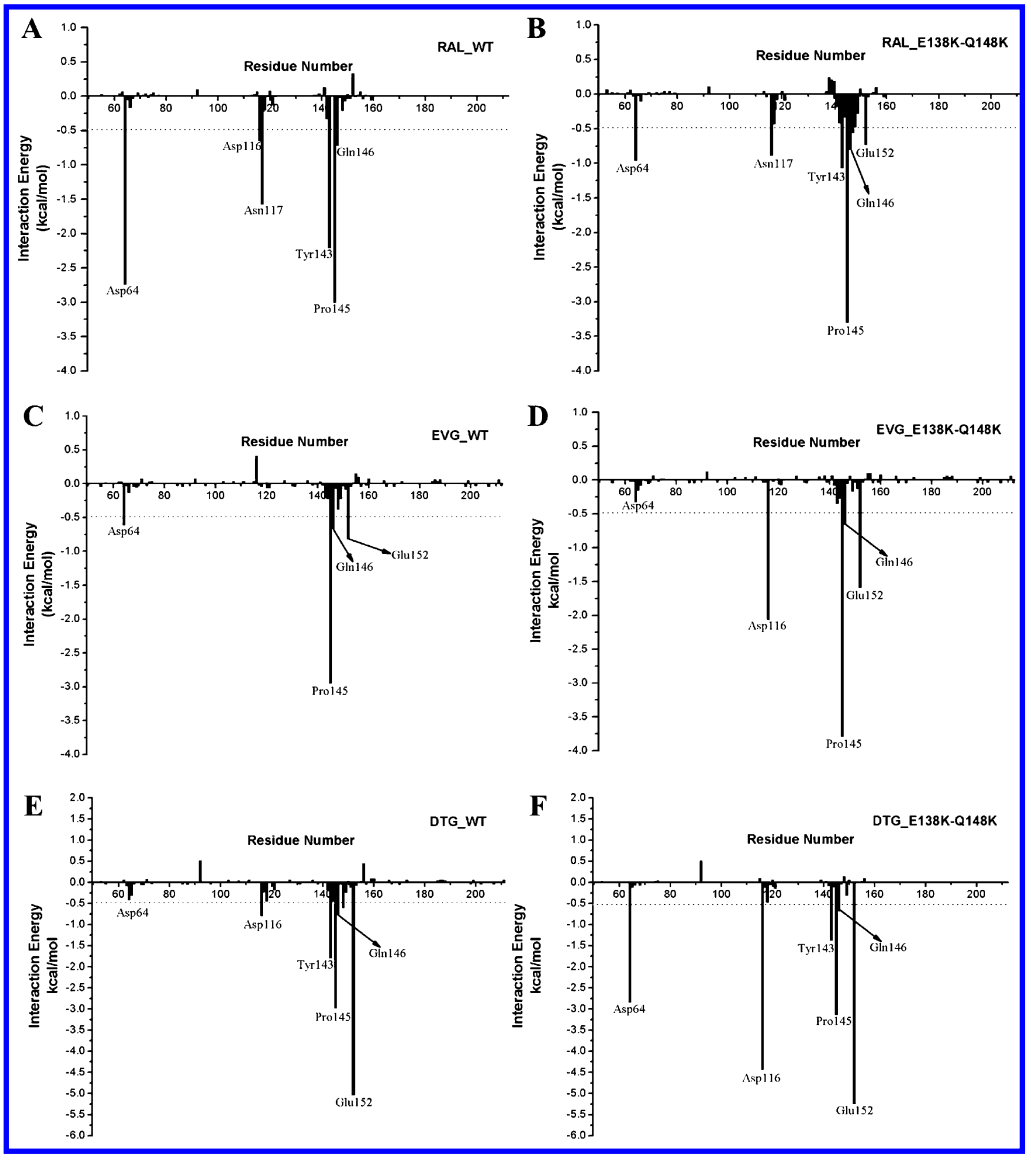

Figure 6. Intermolecular ligand receptor (IN) interaction spectrum of the WT and E138K/Q148K intasome−inhibitor complex according to the MM-GBSA method.

dx.doi.org/10.1021/ci300541c | J. Chem. Inf. Model. 2013, 53, 210−222

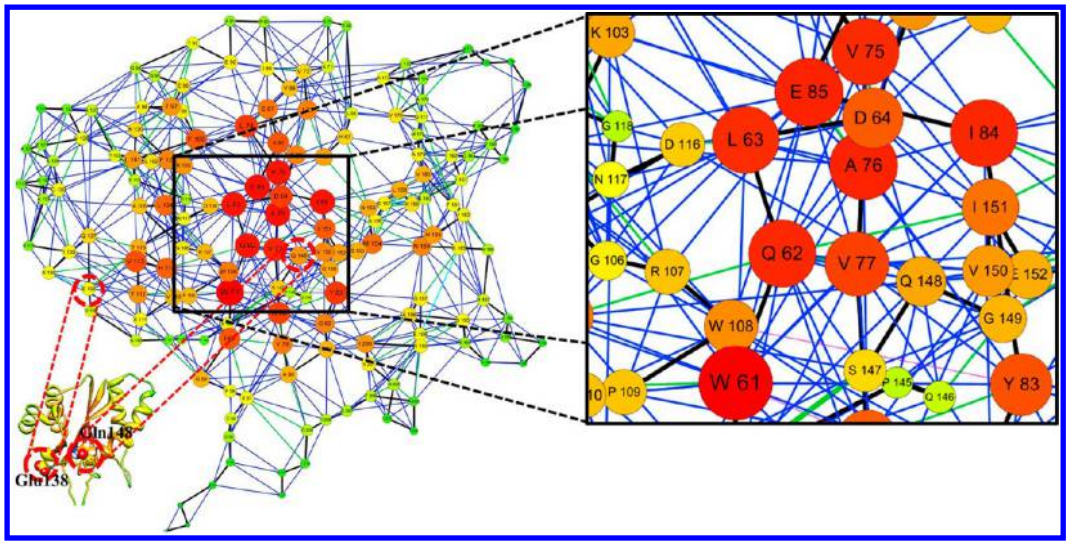

Figure 7. RAL-bound WT HIV-1 IN residue interaction network and its communities. Only the detailed view of noncovalent residue interactions in HIV-1 IN CCD of the network is shown. The edges are colored with respect to their interaction type: backbone (black); interaction between closest atoms (blue); hydrogen bond (green); salt bridge (cyan); π-cation interaction (purple); $\pi-\pi$ interaction (pink). Closeness (shortest path length of to all others) is denoted by nodes color (low values to bright colors). The lower left corner is the simultaneous view of the protein structure in 3D (colored by closeness values) which is provided by UCSF Chimera molecular structure viewer.

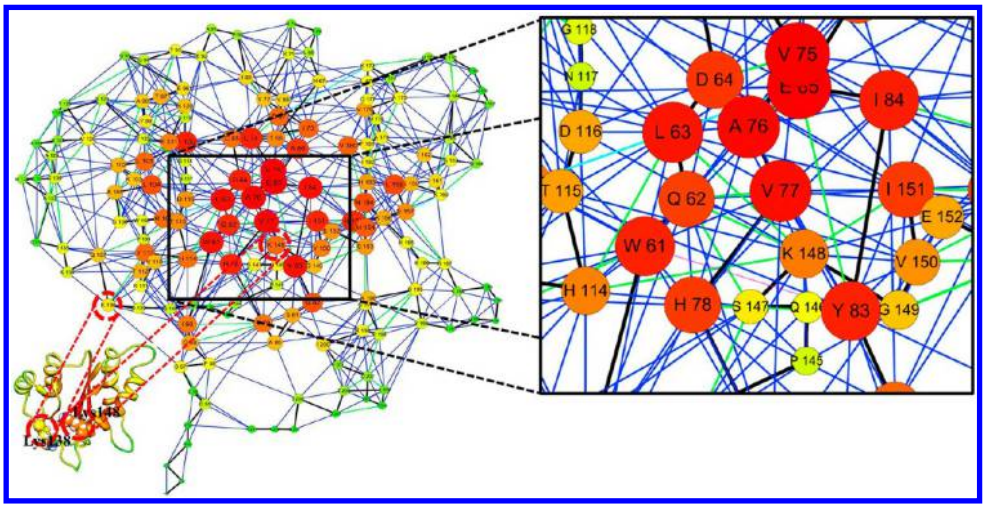

Figure 8. RAL-bound E138K/Q148K HIV-1 IN residue interaction network and its communities. Only the detailed view of noncovalent residue interactions in HIV-1 IN CCD of the network is shown. The edges are colored with respect to their interaction type: backbone (black); interaction between closest atoms (blue); hydrogen bond (green); salt bridge (cyan); π-cation interaction (purple); $\pi-\pi$ interaction (pink). Closeness (shortest path length of to all others) is denoted by node color (low values to bright colors). The lower left corner is the simultaneous view of the protein structure in 3D (colored by closeness values) which is provided by UCSF Chimera molecular structure viewer.

Asp 64 and A17 decreased. However, this mutation induces the contributions from residues Asp116, Glu152, G4, and C16 increased. In particular, the size of the contributions from three catalytic residues Asp64, Asp116, and Glu152 are increased in DTG bound mutant. Because Asp64, Asp116, and Glu152 are well-conserved and important for viral functions, stronger interaction with these residues should help combat resistance. Thus our calculation shows that DTG is more potent against E138K/Q148K mutant when compared with the RAL and EVG. Furthermore, the contribution from residue Pro145 are increased for all INSTIs bound mutant (Figure 6). The contributions of Pro145 for the binding free energy are relevant to the calculated distances between the centroid of INSTIs scaffold and Pro145 in the WT and E138K/Q148K mutant HIV-1 intasome–INSTIs complexes (Table S1, Supporting Information). Little distance change (Table S1, Supporting Information) and binding free energy contribution increase from residue Pro145 was observed for DTG bound complex (Figure 6E and F). Figure 2 illustrates that DTG possesses a less flexible linker region between the metal chelating core and the halogenated phenyl group. This means that the hydrophobic interaction between the Pro145 and INSTIs scaffold is critical to keep the INSTIs in a right conformation to accommodate the HIV-1 intasome active site. The changes of binding free energy contribution of Pro145 are corresponding to the structure rearrangements of the HIV-1 intasome complex active site caused by drug resistance mutation.

Interaction Network and Community of Residues. Exploration and analysis of the residue interaction network (RIN) can give us further insight into the structural and functional role of a residue.[89−91] Recently, RIN analysis has been successfully applied to characterize the effects of residue

dx.doi.org/10.1021/ci300541c | J. Chem. Inf. Model. 2013, 53, 210−222

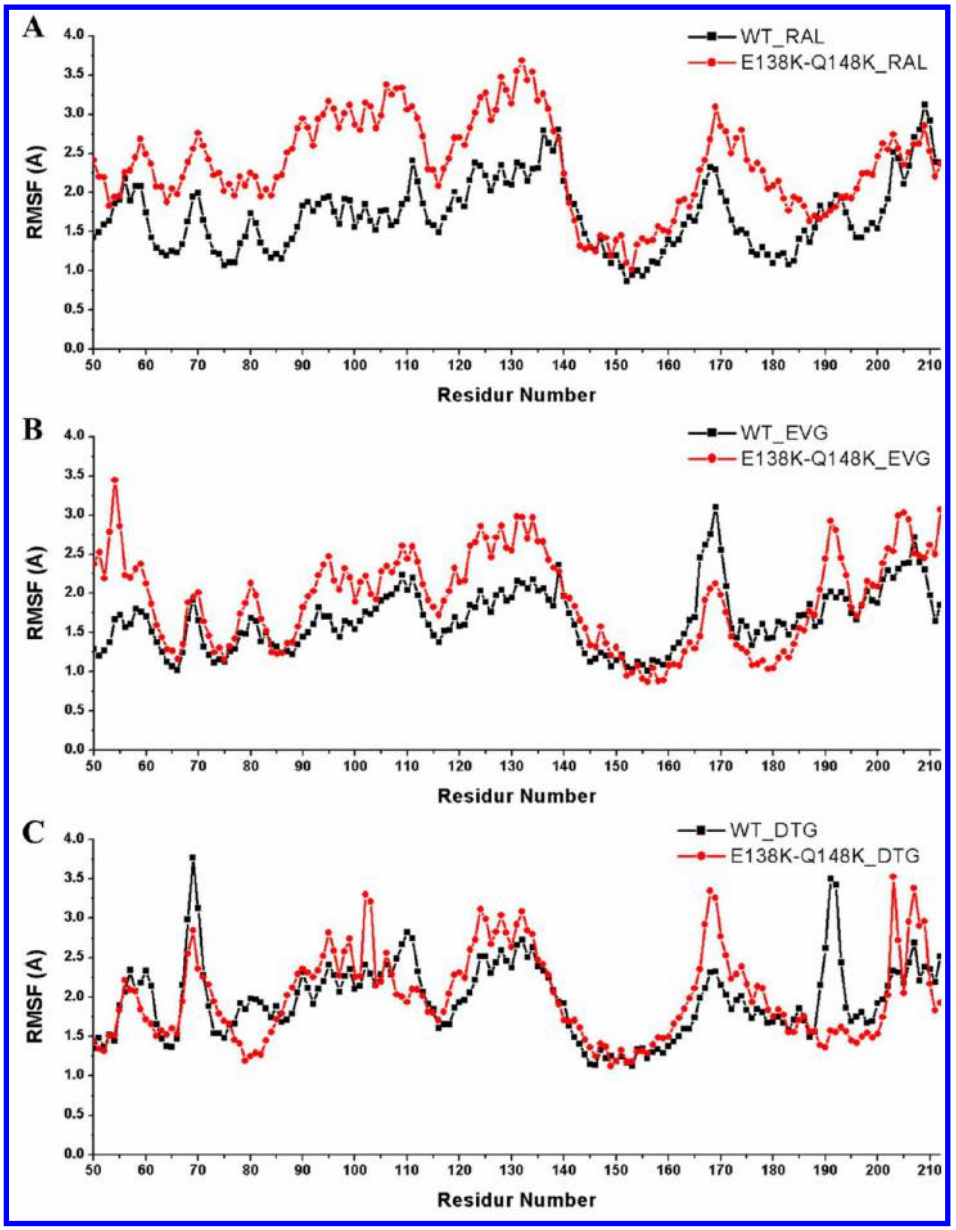

Figure 9. Comparison of the HIV-1 intasome catalytic core domain (CCD) conformational flexibility. The root mean squared fluctuations (RMSF) variations of Cα atoms were calculated. From A−C are represented HIV-1 intasome in complex with RAL, EVG, and DTG. The WT and E138K/Q148K HIV-1 intasome are represented in black and red.

mutation related to drug resistance.[92,93] To explore the cross-resistance mechanism for mutated HIV-1 intasome, we analyzed the information about RIN and the features of the network topologies.

(1) Calculation of RIN. MD simulated protein structures were transformed into 2D representations of residue interaction network by identifying all interactions between the amino acid in each structure. The representations of RIN (Figures 7 and 8 and Figures S2−5 in the Supporting Information) were used to analyze the residue with specific interaction topologies located in the HIV-1 IN CCD. In the RIN, different types of simultaneous noncovalent residue interactions (edges), that is, interaction between closest atoms, hydrogen bond, salt bridge, π-cation interaction, $\pi-\pi$ interaction, and the CCD amino acid residues can be easily identified as the nodes with the number of connections (node degree). In order to further examine the centrality of RIN nodes, we characterize the properties of individual amino acid residues based on their relation with other residues of the protein. RIN centrality measures of individual nodes are based on their distance from other nodes or on their position along paths between other nodes.[94] The distance between two nodes is the number of edges along the shortest path between the nodes.[89] Among the centrality measures, the closeness centrality is a global measure that depends on the whole structure of the protein (RIN). Closeness centrality of a node is the reciprocal of the average shortest path length, and the closeness centrality of each node is a number between 0 and 1.[95] Here we computed the shortest path closeness denoted by nodes color shown in RIN figures with the simultaneous view of the RIN in 2D and the corresponding protein structure in 3D (Figures 7 and 8 and Figures S2−5 in the Supporting Information).

(2) Cross-Resistance Mechanism and Residue Closeness Changes. Communication within protein amino acid residues

dx.doi.org/10.1021/ci300541c | J. Chem. Inf. Model. 2013, 53, 210−222

is crucial for the biological functioning of the protein,[91,96] and closeness centrality is a measure of how quickly information spreads from a given node to other reachable nodes in the network.[95] Previous experimental studies have provided important data that the mutated HIV-1 intasome (E138K/Q148K) caused the decreased affinity of INSTIs (cross-resistance). In Figures 7 and 8 and Figures S2−5 (Supporting Information), we show the residues (nodes) shortest path closeness information about the INSTIs (RAL, EVG, and DTG) bound WT and mutated HIV-1 IN CCD. To get further insight into cross-resistance mechanism in terms of network communications, we compared the RIN for the WT and mutated HIV-1 IN CCD along with their value of closeness are presented in Table S2 (Supporting Information). As observed from Table S2, it is remarkable that the value of closeness for the residues increased significantly in mutated RIN from the RAL- and EVG-bound complexes. Thus, it is evident that, in the mutated HIV-1 intasome, the information spreads from one residue in the protein to other reachable residues more quickly than in the WT complex. Interestingly, there is little increase in the value of the closeness in DTG-bound mutant; meanwhile, a weak cross-resistance profile was observed for DTG. Moreover, based on the results of binding free energy decomposition, the contribution of Pro145 and the distances between the centroid of INSTIs scaffold and Pro145 analysis, we proposed that the Pro145 may play an important role in this information communication in which the E138K/Q148K substitution alters the structure rearrangement in the active site. Here, in order to characterize effect of the E138K/Q148K substitution upon conformational change, we used the root-mean-square fluctuations (RMSF) analysis capable of monitoring the local motion in the protein structure. Application of this analysis to the proteins demonstrated that a higher mobility of the CCD residues of mutants compared with the WT proteins (Figure 9), and the order of predicted RMSF values follows consistently the residue closeness changes. Therefore, the RIN and conformation analysis indicate that there indeed exists a structure rearrangement in E138K/Q148K mutant active site, which will decrease the binding ability of the INSTIs to the active site of HIV-1 intasome.

CONCLUSIONS

In this work, we used a strategy by combing MD simulation and RIN analysis to uncover the molecular mechanism of the cross-resistance mutation E138K/Q148K to three important INSTIs (RAL, EVG, and DTG). This approach reveals that the drug resistance mutation induces an increase of the information communicate ability between CCD residues and further leads to the conformation rearrangement of HIV-1 intasome active site. Furthermore, our study indicates that the active site structure rearrangement alters the two-metal chelating model of RAL and EVG due to the unfavorable orientation of oxygen atoms. Remarkably, a limited cross-resistance profile was observed for the second-generation INSTIs (DTG), which possesses a less flexible linker region between the metal chelating core and the halogenated phenyl group. These findings provide information for understanding the cross-resistance mechanism behind the E138K/Q148K double mutant and will be very useful for the following structure-based design of novel INSTIs less susceptible to drug resistance.

ASSOCIATED CONTENT

Supporting Information

Figure S1: the intermolecular ligand receptor (viral DNA) interaction spectrum of the WT and E138K/Q148K intasome−inhibitor complex. Figure S2−S5: the WT and E138K/Q148K HIV-1 IN residue interaction network and its communities for EVG- and DTG-bound complex. Table S1: the distances between the centroid of INSTIs scaffold and Pro145 in the WT and E138K/Q148K mutant HIV-1 intasome−INSTIs complexes. Table S2 illustrated shortest path closeness values for HIV-1 IN CCD (50−212) in the WT and E138K/Q148K HIV-1 intasome−INSTIs complexes. This material is available free of charge via the Internet at http://pubs.acs.org.

AUTHOR INFORMATION

Corresponding Author

*Tel.: +86-931-891-2578. Fax: +86-931-891-2582. E-mail: xjyao@lzu.edu.cn.

Notes

The authors declare no competing financial interest.

ACKNOWLEDGMENTS

This work was supported by the National Natural Science Foundation of China (Grant Nos. 20905033, 21175063), the Program for New Century Excellent Talents in University (Grant No. NCET-07-0399), and the Fundamental Research Funds for the Central Universities (Grant Nos. lzujbky-2011-19, lzujbky-2012-k10).

REFERENCES

(1) Barre-Sinoussi, F.; Chermann, J.; Rey, F.; Nugeyre, M.; Chamaret, S.; Gruest, J.; Dauguet, C.; Axler-Blin, C.; Vezinet-Brun, F.; Rouzioux, C.; Rozenbaum, W.; Montagnier, L. Isolation of a T-lymphotropic retrovirus from a patient at risk for acquired immune deficiency syndrome (AIDS). *Science* **1983**, *220*, 868−871.

(2) Schupbach, J.; Popovic, M.; Gilden, R.; Gonda, M.; Sarngadharan, M.; Gallo, R. Serological analysis of a subgroup of human T-lymphotropic retroviruses (HTLV-III) associated with AIDS. *Science* **1984**, *224*, 503−505.

(3) Weiss, R. How does HIV cause AIDS? *Science* **1993**, *260*, 1273−1279.

(4) Hammer Sm, S. M. S. S. M.; et al. Treatment for adult hiv infection: 2006 recommendations of the international aids society−usa panel. *J. Am. Med. Assoc.* **2006**, *296*, 827−843.

(5) Douek, D. C.; Roederer, M.; Koup, R. A. Emerging Concepts in the Immunopathogenesis of AIDS. *Annu. Rev. Med.* **2009**, *60*, 471−484.

(6) Goldgur, Y.; Craigie, R.; Cohen, G. H.; Fujiwara, T.; Yoshinaga, T.; Fujishita, T.; Sugimoto, H.; Endo, T.; Murai, H.; Davies, D. R. Structure of the HIV-1 integrase catalytic domain complexed with an inhibitor: A platform for antiviral drug design. *Proc. Natl. Acad. Sci.* **1999**, *96*, 13040−13043.

(7) Schames, J. R.; Henchman, R. H.; Siegel, J. S.; Sotriffer, C. A.; Ni, H.; McCammon, J. A. Discovery of a Novel Binding Trench in HIV Integrase. *J. Med. Chem.* **2004**, *47*, 1879−1881.

(8) Summa, V.; Petrocchi, A.; Bonelli, F.; Crescenzi, B.; Donghi, M.; Ferrara, M.; Fiore, F.; Gardelli, C.; Gonzalez Paz, O.; Hazuda, D. J.; Jones, P.; Kinzel, O.; Laufer, R.; Monteagudo, E.; Muraglia, E.; Nizi, E.; Orvieto, F.; Pace, P.; Pescatore, G.; Scarpelli, R.; Stillmock, K.; Witmer, M. V.; Rowley, M. Discovery of Raltegravir, a Potent, Selective Orally Bioavailable HIV-Integrase Inhibitor for the Treatment of HIV-AIDS Infection. *J. Med. Chem.* **2008**, *51*, 5843−5855.

(9) Asante-Appiah, E.; Skalka, A. M. HIV-1 Integrase: Structural Organization, Conformational Changes, and Catalysis. In *Advances in*

Virus Research; Karl Rlaramorosch, F. A. M.; Aaron, J. S., Eds.; Academic Press: Philadelphia, 1999; pp 351−369.
(10) Engelman, A.; Hickman, A. B.; Craigie, R. The core and carboxyl-terminal domains of the integrase protein of human immunodeficiency virus type 1 each contribute to nonspecific DNA binding. *J. Virol.* **1994**, *68*, 5911−5917.
(11) Kukolj, G.; Skalka, A. M. Enhanced and coordinated processing of synapsed viral DNA ends by retroviral integrases in vitro. *Gene. Dev.* **1995**, *9*, 2556−2567.
(12) Cahn, P.; Sued, O. Raltegravir: a new antiretroviral class for salvage therapy. *The Lancet* **2007**, *369*, 1235−1236.
(13) DeJesus, E.; Berger, D.; Markowitz, M.; Cohen, C.; Hawkins, T.; Ruane, P.; Elion, R.; Farthing, C.; Zhong, L.; Cheng, A. K.; McColl, D.; Kearney, B. P. Team, f. t.-S. Antiviral Activity, Pharmacokinetics, and Dose Response of the HIV-1 Integrase Inhibitor GS-9137 (JTK-303) in Treatment-Naive and Treatment-Experienced Patients. *J. Acquir. Immune Defic. Syndr.* **2006**, *43*, 1−5.
(14) Kobayashi, M.; Yoshinaga, T.; Seki, T.; Wakasa-Morimoto, C.; Brown, K. W.; Ferris, R.; Foster, S. A.; Hazen, R. J.; Miki, S.; Suyama-Kagitani, A.; Kawauchi-Miki, S.; Taishi, T.; Kawasuji, T.; Johns, B. A.; Underwood, M. R.; Garvey, E. P.; Sato, A.; Fujiwara, T. In Vitro Antiretroviral Properties of S/GSK1349572, a Next-Generation HIV Integrase Inhibitor. *Antimicrob. Agents Chemother.* **2011**, *55*, 813−821.
(15) Lenz, J. C. C.; Rockstroh, J. K. S/GSK1349572, a new integrase inhibitor for the treatment of HIV: promises and challenges. *Expert. Opin. Investig. Drugs* **2011**, *20*, 537−548.
(16) Koelsch, K. K.; Cooper, D. A. Integrase inhibitors in salvage therapy regimens for HIV-1 infection. *Curr. Opin. HIV AIDS* **2009**, *4*, 518−523.
(17) Hill, A. New Quad HIV pill on track for FDA approval. http://www.inpharm.com/news/172624/new-quad-hiv-pill-track-fda-approval (accessed Nov 25, 2012).
(18) Marchand, C. The elvitegravir Quad pill: the first once-daily dual-target anti-HIV tablet. *Expert. Opin. Investig. Drugs* **2012**, *21*, 901−904.
(19) Yin, Z.; Craigie, R. Modeling the HIV-1 Intasome: A Prototype View of the Target of Integrase Inhibitors. *Viruses* **2010**, *2*, 2777−2781.
(20) Marchand, C.; Maddali, K.; Metifiot, M.; Pommier, Y. HIV-1 IN Inhibitors: 2010 Update and Perspectives. *Curr. Top. Med. Chem.* **2009**, *9*, 1016−1037.
(21) Blanco, J.-L.; Varghese, V.; Rhee, S.-Y.; Gatell, J. M.; Shafer, R. W. HIV-1 Integrase Inhibitor Resistance and Its Clinical Implications. *J. Infect. Dis.* **2011**, *203*, 1204−1214.
(22) Marinello, J.; Marchand, C.; Mott, B. T.; Bain, A.; Thomas, C. J.; Pommier, Y. Comparison of Raltegravir and Elvitegravir on HIV-1 Integrase Catalytic Reactions and on a Series of Drug-Resistant Integrase Mutants. *Biochemistry* **2008**, *47*, 9345−9354.
(23) Van Wesenbeeck, L.; Rondelez, E.; Feyaerts, M.; Verheyen, A.; Van der Borght, K.; Smits, V.; Cleybergh, C.; De Wolf, H.; Van Baelen, K.; Stuyver, L. J. Cross-Resistance Profile Determination of Two Second-Generation HIV-1 Integrase Inhibitors Using a Panel of Recombinant Viruses Derived from Raltegravir-Treated Clinical Isolates. *Antimicrob. Agents Chemother.* **2011**, *55*, 321−325.
(24) Canducci, F.; Ceresola, E. R.; Boeri, E.; Spagnuolo, V.; Cossarini, F.; Castagna, A.; Lazzarin, A.; Clementi, M. Cross-resistance Profile of the Novel Integrase Inhibitor Dolutegravir (S/GSK1349572) Using Clonal Viral Variants Selected in Patients Failing Raltegravir. *J. Infect. Dis.* **2011**, *204*, 1811−1815.
(25) Barreca, M. L.; Lee, K. W.; Chimirri, A.; Briggs, J. M. Molecular Dynamics Studies of the Wild-Type and Double Mutant HIV-1 Integrase Complexed with the 5CITEP Inhibitor: Mechanism for Inhibition and Drug Resistance. *Biophys. J.* **2003**, *84*, 1450−1463.
(26) Williams, S. L.; Essex, J. W. Study of the Conformational Dynamics of the Catalytic Loop of WT and G140A/G149A HIV-1 Integrase Core Domain Using Reversible Digitally Filtered Molecular Dynamics. *J. Chem. Theory Comput.* **2009**, *5*, 411−421.
(27) Sippel, M.; Sotriffer, C. A. Molecular Dynamics Simulations of the HIV-1 Integrase Dimerization Interface: Guidelines for the Design of a Novel Class of Integrase Inhibitors. *J. Chem. Inf. Model.* **2010**, *50*, 604−614.
(28) Perryman, A. L.; Forli, S.; Morris, G. M.; Burt, C.; Cheng, Y.; Palmer, M. J.; Whitby, K.; McCammon, J. A.; Phillips, C.; Olson, A. J. A Dynamic Model of HIV Integrase Inhibition and Drug Resistance. *J. Mol. Biol.* **2010**, *397*, 600−615.
(29) Huang, M.; Grant, G. H.; Richards, W. G. Binding modes of diketo-acid inhibitors of HIV-1 integrase: A comparative molecular dynamics simulation study. *J. Mol. Graph. Model.* **2011**, *29*, 956−964.
(30) Chen, H.; Wei, S.-Q.; Engelman, A. Multiple Integrase Functions Are Required to Form the Native Structure of the Human Immunodeficiency Virus Type I Intasome. *J. Biol. Chem.* **1999**, *274*, 17358−17364.
(31) Li, M.; Mizuuchi, M.; Burke, T. R.; Craigie, R. Retroviral DNA integration: reaction pathway and critical intermediates. *Embo. J.* **2006**, *25*, 1295−1304.
(32) Krishnan, L.; Li, X.; Naraharisetty, H. L.; Hare, S.; Cherepanov, P.; Engelman, A. Structure-based modeling of the functional HIV-1 intasome and its inhibition. *Proc. Natl. Acad. Sci.* **2010**, *107*, 15910−15915.
(33) Xue, W.; Liu, H.; Yao, X. Molecular mechanism of HIV-1 integrase-vDNA interactions and strand transfer inhibitor action: A molecular modeling perspective. *J. Comput. Chem.* **2012**, *33*, 527−536.
(34) Hazuda, D. J. Resistance to inhibitors of the human immunodeficiency virus type 1 integration. *Braz. J. Infect. Dis.* **2010**, *14*, 513−518.
(35) Hare, S.; Gupta, S. S.; Valkov, E.; Engelman, A.; Cherepanov, P. Retroviral intasome assembly and inhibition of DNA strand transfer. *Nature* **2010**, *464*, 232−236.
(36) Hare, S.; Vos, A. M.; Clayton, R. F.; Thuring, J. W.; Cummings, M. D.; Cherepanov, P. Molecular mechanisms of retroviral integrase inhibition and the evolution of viral resistance. *Proc. Natl. Acad. Sci.* **2010**, *107*, 20057−20062.
(37) Métifiot, M.; Johnson, B.; Smith, S.; Zhao, X. Z.; Marchand, C.; Burke, T.; Hughes, S.; Pommier, Y. MK-0536 Inhibits HIV-1 Integrases Resistant to Raltegravir. *Antimicrob. Agents Chemother.* **2011**, *55*, 5127−5133.
(38) Johnson, B. C.; Metifiot, M.; Pommier, Y.; Hughes, S. H. Molecular Dynamics Approaches Estimate the Binding Energy of HIV-1 Integrase Inhibitors and Correlate with In Vitro Activity. *Antimicrob. Agents Chemother.* **2012**, *56*, 411−419.
(39) Xue, W.; Qi, J.; Yang, Y.; Jin, X.; Liu, H.; Yao, X. Understanding the effect of drug-resistant mutations of HIV-1 intasome on raltegravir action through molecular modeling study. *Mol. Biosyst.* **2012**, *8*, 2135−2144.
(40) Hare, S.; Vos, A. M.; Clayton, R. F.; Thuring, J. W.; Cummings, M. D.; Cherepanov, P. Molecular mechanisms of retroviral integrase inhibition and the evolution of viral resistance. *Proc. Natl. Acad. Sci.* **2010**, *107*, 20057−20062.
(41) Humphrey, W.; Dalke, A.; Schulten, K. VMD: Visual molecular dynamics. *J. Mol. Graph.* **1996**, *14*, 33−38.
(42) Hare, S.; Smith, S. J.; Métifiot, M.; Jaxa-Chamiec, A.; Pommier, Y.; Hughes, S. H.; Cherepanov, P. Structural and Functional Analyses of the Second-Generation Integrase Strand Transfer Inhibitor Dolutegravir (S/GSK1349572). *Mol. Pharmacol.* **2011**, *80*, 565−572.
(43) Guex, N.; Peitsch, M. C. SWISS-MODEL and the Swiss-Pdb Viewer: An environment for comparative protein modeling. *Electrophoresis* **1997**, *18*, 2714−2723.
(44) *The PyMOL Molecular Graphics System*, Version 0.99rc6; DeLano Scientific LLC: Palo Alto, CA. 2008.
(45) Case, D. A.; Darden, T. A.; Cheatham, T. E. III; Simmerling, C. L.; Wang, J.; Duke, R. E.; Luo, R.; Crowley, M.; Walker, R. C.; Zhang, W.; Merz, K. M.; Wang, B.; Hayik, S.; Roitberg, A.; Seabra, G.; Kolossváry, I.; Wong, K. F.; Paesani, F.; Vanicek, J.; Wu, X.; Brozell, S. R.; Steinbrecher, T.; Gohlke, H.; Yang, L.; Tan, C.; Mongan, J.; Hornak, V.; Cui, G.; Mathews, D. H.; Seetin, M. G.; Sagui, C.; Babin, V.; Kollman, P. A. AMBER 10; University of California, San Francisco, 2008.

(46) Jorgensen, W. L.; Chandrasekhar, J.; Madura, J. D.; Impey, R. W.; Klein, M. L. Comparison of simple potential functions for simulating liquid water. *J. Chem. Phys.* **1983**, *79*, 926−935.
(47) Duan, Y.; Wu, C.; Chowdhury, S.; Lee, M. C.; Xiong, G.; Zhang, W.; Yang, R.; Cieplak, P.; Luo, R.; Lee, T.; Caldwell, J.; Wang, J.; Kollman, P. A point-charge force field for molecular mechanics simulations of proteins based on condensed-phase quantum mechanical calculations. *J. Comput. Chem.* **2003**, *24*, 1999−2012.
(48) Stote, R. H.; Karplus, M. Zinc binding in proteins and solution: A simple but accurate nonbonded representation. *Proteins: Struct. Funct. Bioinform.* **1995**, *23*, 12−31.
(49) Wang, J.; Wolf, R. M.; Caldwell, J. W.; Kollman, P. A.; Case, D. A. Development and testing of a general amber force field. *J. Comput. Chem.* **2004**, *25*, 1157−1174.
(50) Bayly, C. I.; Cieplak, P.; Cornell, W.; Kollman, P. A. A well-behaved electrostatic potential based method using charge restraints for deriving atomic charges: the RESP model. *J. Phys. Chem.* **1993**, *97*, 10269−10280.
(51) Cieplak, P.; Cornell, W. D.; Bayly, C.; Kollman, P. A. Application of the multimolecule and multiconformational RESP methodology to biopolymers: Charge derivation for DNA, RNA, and proteins. *J. Comput. Chem.* **1995**, *16*, 1357−1377.
(52) Fox, T.; Kollman, P. A. Application of the RESP Methodology in the Parametrization of Organic Solvents. *J. Phys. Chem. B* **1998**, *102*, 8070−8079.
(53) Frisch, M. J.; Trucks, G. W.; Schlegel, H. B.; Scuseria, G. E.; Robb, M. A.; Cheeseman, J. R.; Scalmani, G.; Barone, V.; Mennucci, B.; Petersson, G. A.; Nakatsuji, H.; Caricato, M.; Li, X.; Hratchian, H. P.; Izmaylov, A. F.; Bloino, J.; Zheng, G.; Sonnenberg, J. L.; Hada, M.; Ehara, M.; Toyota, K.; Fukuda, R.; Hasegawa, J.; Ishida, M.; Nakajima, T.; Honda, Y.; Kitao, O.; Nakai, H.; Vreven, T.; Montgomery, J. A., Jr.; Peralta, J. E.; Ogliaro, F.; Bearpark, M.; Heyd, J. J.; Brothers, E.; Kudin, K. N.; Staroverov, V. N.; Kobayashi, R.; Normand, J.; Raghavachari, K.; Rendell, A.; Burant, J. C.; Iyengar, S. S.; Tomasi, J.; Cossi, M.; Rega, N.; Millam, N. J.; Klene, M.; Knox, J. E.; Cross, J. B.; Bakken, V.; Adamo, C.; Jaramillo, J.; Gomperts, R.; Stratmann, R. E.; Yazyev, O.; Austin, A. J.; Cammi, R.; Pomelli, C.; Ochterski, J. W.; Martin, R. L.; Morokuma, K.; Zakrzewski, V. G.; Voth, G. A.; Salvador, P.; Dannenberg, J. J.; Dapprich, S.; Daniels, A. D.; Farkas, Ö.; Foresman, J. B.; Ortiz, J. V.; Cioslowski, J.; Fox, D. J. Gaussian 09; Gaussian, Inc.: Wallingford, CT, 2009.
(54) Darden, T.; York, D.; Pedersen, L. Particle mesh Ewald: An N·log(N) method for Ewald sums in large systems. *J. Chem. Phys.* **1993**, *98*, 10089−10092.
(55) Ryckaert, J.-P.; Ciccotti, G.; Berendsen, H. J. C. Numerical integration of the cartesian equations of motion of a system with constraints: molecular dynamics of n-alkanes. *J. Comput. Phys.* **1977**, *23*, 327−341.
(56) Kollman, P. A.; Massova, I.; Reyes, C.; Kuhn, B.; Huo, S.; Chong, L.; Lee, M.; Lee, T.; Duan, Y.; Wang, W.; Donini, O.; Cieplak, P.; Srinivasan, J.; Case, D. A.; Cheatham, T. E. Calculating Structures and Free Energies of Complex Molecules: Combining Molecular Mechanics and Continuum Models. *Acc. Chem. Res.* **2000**, *33*, 889−897.
(57) Massova, I.; Kollman, P. Combined molecular mechanical and continuum solvent approach (MM-PBSA/GBSA) to predict ligand binding. *Perspect. Drug Discov.* **2000**, *18*, 113−135.
(58) Tsui, V.; Case, D. A. Theory and applications of the generalized born solvation model in macromolecular simulations. *Biopolymers* **2000**, *56*, 275−291.
(59) Onufriev, A.; Bashford, D.; Case, D. A. Modification of the Generalized Born Model Suitable for Macromolecules. *J. Phys. Chem. B* **2000**, *104*, 3712−3720.
(60) Gohlke, H.; Kiel, C.; Case, D. A. Insights into Protein-Protein Binding by Binding Free Energy Calculation and Free Energy Decomposition for the Ras-Raf and Ras-RalGDS Complexes. *J. Mol. Biol.* **2003**, *330*, 891−913.
(61) Rizzo, R. C.; Toba, S.; Kuntz, I. D. A Molecular Basis for the Selectivity of Thiadiazole Urea Inhibitors with Stromelysin-1 and Gelatinase-A from Generalized Born Molecular Dynamics Simulations. *J. Med. Chem.* **2004**, *47*, 3065−3074.
(62) Kormos, B. L.; Benitex, Y.; Baranger, A. M.; Beveridge, D. L. Affinity and Specificity of Protein U1A-RNA Complex Formation Based on an Additive Component Free Energy Model. *J. Mol. Biol.* **2007**, *371*, 1405−1419.
(63) Hou, T.; Yu, R. Molecular Dynamics and Free Energy Studies on the Wild-type and Double Mutant HIV-1 Protease Complexed with Amprenavir and Two Amprenavir-Related Inhibitors: Mechanism for Binding and Drug Resistance. *J. Med. Chem.* **2007**, *50*, 1177−1188.
(64) Chachra, R.; Rizzo, R. C. Origins of Resistance Conferred by the R292K Neuraminidase Mutation via Molecular Dynamics and Free Energy Calculations. *J. Chem. Theory Comput.* **2008**, *4*, 1526−1540.
(65) Hou, T.; Zhang, W.; Wang, J.; Wang, W. Predicting drug resistance of the HIV-1 protease using molecular interaction energy components. *Proteins: Struct. Funct. Bioinform.* **2009**, *74*, 837−846.
(66) Liu, H.; Yao, X.; Wang, C.; Han, J. In Silico Identification of the Potential Drug Resistance Sites over 2009 Influenza A (H1N1) Virus Neuraminidase. *Mol. Pharmaceutics* **2010**, *7*, 894−904.
(67) Xue, W.; Pan, D.; Yang, Y.; Liu, H.; Yao, X. Molecular modeling study on the resistance mechanism of HCV NS3/4A serine protease mutants R155K, A156V and D168A to TMC435. *Antiviral Res.* **2012**, *93*, 126−137.
(68) Sitkoff, D.; Sharp, K. A.; Honig, B. Accurate Calculation of Hydration Free Energies Using Macroscopic Solvent Models. *J. Phys. Chem.* **1994**, *98*, 1978−1988.
(69) Pearlman, D. A.; Case, D. A.; Caldwell, J. W.; Ross, W. S.; Cheatham, T. E., Iii; DeBolt, S.; Ferguson, D.; Seibel, G.; Kollman, P. AMBER, a package of computer programs for applying molecular mechanics, normal mode analysis, molecular dynamics and free energy calculations to simulate the structural and energetic properties of molecules. *Comput. Phys. Commun.* **1995**, *91*, 1−41.
(70) Onufriev, A.; Bashford, D.; Case, D. A. Exploring protein native states and large-scale conformational changes with a modified generalized born model. *Proteins: Struct. Funct. Bioinform.* **2004**, *55*, 383−394.
(71) Word, J. M.; Lovell, S. C.; Richardson, J. S.; Richardson, D. C. Asparagine and glutamine: using hydrogen atom contacts in the choice of side-chain amide orientation. *J. Mol. Biol.* **1999**, *285*, 1735−1747.
(72) Word, J. M.; Lovell, S. C.; LaBean, T. H.; Taylor, H. C.; Zalis, M. E.; Presley, B. K.; Richardson, J. S.; Richardson, D. C. Visualizing and quantifying molecular goodness-of-fit: small-probe contact dots with explicit hydrogen atoms. *J. Mol. Biol.* **1999**, *285*, 1711−1733.
(73) Shannon, P.; Markiel, A.; Ozier, O.; Baliga, N. S.; Wang, J. T.; Ramage, D.; Amin, N.; Schwikowski, B.; Ideker, T. Cytoscape: A Software Environment for Integrated Models of Biomolecular Interaction Networks. *Genome Res.* **2003**, *13*, 2498−2504.
(74) Doncheva, N. T.; Klein, K.; Domingues, F. S.; Albrecht, M. Analyzing and visualizing residue networks of protein structures. *Trends. Biochem. Sci.* **2011**, *36*, 179−182.
(75) Assenov, Y.; Ramírez, F.; Schelhorn, S.-E.; Lengauer, T.; Albrecht, M. Computing topological parameters of biological networks. *Bioinformatics* **2008**, *24*, 282−284.
(76) Jenkins, T. M.; Hickman, A. B.; Dyda, F.; Ghirlando, R.; Davies, D. R.; Craigie, R. Catalytic domain of human immunodeficiency virus type 1 integrase: identification of a soluble mutant by systematic replacement of hydrophobic residues. *Proc. Natl. Acad. Sci.* **1995**, *92*, 6057−6061.
(77) Barreca, M. L.; Ferro, S.; Rao, A.; De Luca, L.; Zappalà, M.; Monforte, A.-M.; Debyser, Z.; Witvrouw, M.; Chimirri, A. Pharmacophore-Based Design of HIV-1 Integrase Strand-Transfer Inhibitors. *J. Med. Chem.* **2005**, *48*, 7084−7088.
(78) Zhao, X. Z.; Maddali, K.; Christie Vu, B.; Marchand, C.; Hughes, S. H.; Pommier, Y.; Burke, T. R., Jr Examination of halogen substituent effects on HIV-1 integrase inhibitors derived from 2,3-dihydro-6,7-dihydroxy-1H-isoindol-1-ones and 4,5-dihydroxy-1H-isoindole-1,3(2H)-diones. *Bioorg. Med. Chem. Lett.* **2009**, *19*, 2714−2717.
(79) Goethals, O.; Vos, A.; Van Ginderen, M.; Geluykens, P.; Smits, V.; Schols, D.; Hertogs, K.; Clayton, R. Primary mutations selected in

vitro with raltegravir confer large fold changes in susceptibility to first-generation integrase inhibitors, but minor fold changes to inhibitors with second-generation resistance profiles. *Virology* **2010**, *402*, 338−346.
(80) Bar-Magen, T.; Sloan, R. D.; Donahue, D. A.; Kuhl, B. D.; Zabeida, A.; Xu, H.; Oliveira, M.; Hazuda, D. J.; Wainberg, M. A. Identification of Novel Mutations Responsible for Resistance to MK-2048, a Second-Generation HIV-1 Integrase Inhibitor. *J. Virol.* **2010**, *84*, 9210−9216.
(81) Langley, D. R.; Samanta, H. K.; Lin, Z.; Walker, M. A.; Krystal, M. R.; Dicker, I. B. The Terminal (Catalytic) Adenosine of the HIV LTR Controls the Kinetics of Binding and Dissociation of HIV Integrase Strand Transfer Inhibitors. *Biochemistry* **2008**, *47*, 13481−13488.
(82) Kijama, R.; Kawasuji, T. *Dual Divalent Metal Ion Chelators as HIV Integrase Inhibitors*. Patent WO 01/95905, Assignee: Shionogi & Co., Ltd., 2001.
(83) Grobler, J. A.; Stillmock, K.; Hu, B.; Witmer, M.; Felock, P.; Espeseth, A. S.; Wolfe, A.; Egbertson, M.; Bourgeois, M.; Melamed, J.; Wai, J. S.; Young, S.; Vacca, J.; Hazuda, D. J. Diketo acid inhibitor mechanism and HIV-1 integrase: Implications for metal binding in the active site of phosphotransferase enzymes. *Proc. Natl. Acad. Sci.* **2002**, *99*, 6661−6666.
(84) Hazuda, D. J.; Anthony, N. J.; Gomez, R. P.; Jolly, S. M.; Wai, J. S.; Zhuang, L.; Fisher, T. E.; Embrey, M.; Guare, J. P.; Egbertson, M. S.; Vacca, J. P.; Huff, J. R.; Felock, P. J.; Witmer, M. V.; Stillmock, K. A.; Danovich, R.; Grobler, J.; Miller, M. D.; Espeseth, A. S.; Jin, L.; Chen, I.-W.; Lin, J. H.; Kassahun, K.; Ellis, J. D.; Wong, B. K.; Xu, W.; Pearson, P. G.; Schleif, W. A.; Cortese, R.; Emini, E.; Summa, V.; Holloway, M. K.; Young, S. D. A naphthyridine carboxamide provides evidence for discordant resistance between mechanistically identical inhibitors of HIV-1 integrase. *Proc. Natl. Acad. Sci.* **2004**, *101*, 11233−11238.
(85) Kawasuji, T.; Fuji, M.; Yoshinaga, T.; Sato, A.; Fujiwara, T.; Kiyama, R. A platform for designing HIV integrase inhibitors. Part 2: A two-metal binding model as a potential mechanism of HIV integrase inhibitors. *Bioorg. Med. Chem.* **2006**, *14*, 8420−8429.
(86) Bacchi, A.; Carcelli, M.; Compari, C.; Fisicaro, E.; Pala, N.; Rispoli, G.; Rogolino, D.; Sanchez, T. W.; Sechi, M.; Neamati, N. HIV-1 IN Strand Transfer Chelating Inhibitors: A Focus on Metal Binding. *Mol. Pharm.* **2011**, *8*, 507−519.
(87) Agrawal, A.; DeSoto, J.; Fullagar, J. L.; Maddali, K.; Rostami, S.; Richman, D. D.; Pommier, Y.; Cohen, S. M. Probing chelation motifs in HIV integrase inhibitors. *Proc. Natl. Acad. Sci.* **2012**, *109*, 2251−2256.
(88) Tang, J.; Maddali, K.; Metifiot, M.; Sham, Y. Y.; Vince, R.; Pommier, Y.; Wang, Z. 3-Hydroxypyrimidine-2,4-diones as an Inhibitor Scaffold of HIV Integrase. *J. Med. Chem.* **2011**, *54*, 2282−2292.
(89) Amitai, G.; Shemesh, A.; Sitbon, E.; Shklar, M.; Netanely, D.; Venger, I.; Pietrokovski, S. Network Analysis of Protein Structures Identifies Functional Residues. *J. Mol. Biol.* **2004**, *344*, 1135−1146.
(90) del Sol, A.; Fujihashi, H.; Amoros, D.; Nussinov, R. Residues crucial for maintaining short paths in network communication mediate signaling in proteins. *Mol. Syst. Biol.* **2006**, *2*, 2006.0019.
(91) Vishveshwara, S. Intra and Inter-Molecular Communications Through Protein Structure. *Curr. Protein Pept. Sci.* **2009**, *10*, 146−160.
(92) Welsch, C.; Domingues, F.; Susser, S.; Antes, I.; Hartmann, C.; Mayr, G.; Schlicker, A.; Sarrazin, C.; Albrecht, M.; Zeuzem, S.; Lengauer, T. Molecular basis of telaprevir resistance due to V36 and T54 mutations in the NS3−4A protease of the hepatitis C virus. *Genome Biol.* **2008**, *9*, R16.
(93) Welsch, C.; Schweizer, S.; Shimakami, T.; Domingues, F. S.; Kim, S.; Lemon, S. M.; Antes, I. Ketoamide Resistance and Hepatitis C Virus Fitness in Val55 Variants of the NS3 Serine Protease. *Antimicrob. Agents Chemother.* **2012**, *56*, 1907−1915.
(94) Freeman, L. Centrality in valued graphs: A measure of betweenness based on network flow. *Social Networks* **1991**, *13*, 141−154.
(95) Freeman, L. C. Centrality in social networks conceptual clarification. *Social Networks* **1978**, *1*, 215−239.
(96) Suel, G. M.; Lockless, S. W.; Wall, M. A.; Ranganathan, R. Evolutionarily conserved networks of residues mediate allosteric communication in proteins. *Nat. Struct. Mol. Biol.* **2003**, *10*, 59−69.